Optimal Trajectories for Planetary Pole-Sitter Missions

Mike Walmsley[1]
University of Edinburgh, United Kingdom

Jeannette Heiligers[2]
Delft University of Technology, the Netherlands

and

Matteo Ceriotti[3] and Colin McInnes[4]
University of Glasgow, United Kingdom

I. Introduction

The pole-sitter [1] is a spacecraft that is stationary on the Earth's axis of rotation, achieving constant coverage of the high latitudes, and enabling unique applications such as geoscience monitoring, improved high-latitude weather prediction and telecommunications [2]. The concept adds to the trade-off between observational revisit time (or temporal resolution) and spatial resolution currently made in designing satellite missions for study of Earth's North or South Poles. However, continuous propulsion is required to maintain this non-Keplerian orbit and past studies have shown that it can be provided by either a solar electric propulsion (SEP) thruster [1] or a hybrid of SEP and solar sailing [3].

Solar sailing is a relatively new form of low-thrust propulsion that employs a large, thin and highly reflective membrane to reflect photons, thereby producing a thrust [4]. Successful deployment and navigation of such a sail in space has recently been achieved with the IKAROS [5], NanoSail-D2 [6] and LightSail-1 [7] missions. For the pole-sitter concept, it has been shown that, by adding this propellantless type of propulsion to an SEP spacecraft, a reduction in propellant consumption can be achieved, thereby increasing the mission lifetime and/or payload mass [3].

Previous work [8] has demonstrated the potential of this novel propulsion system for Earth pole-sitters, which is extended in this Note to pole-sitters above other planets' Poles [9]. Enabling such a vantage point, for example, at Mars can enable unique applications such as continuous communication with Earth during Martian occultation or as a

[1] Undergraduate, School of Physics and Astronomy, James Clerk Maxwell Building, Edinburgh, EH9 3FD s1220970@sms.ed.ac.uk
[2] Marie Skłodowska-Curie Research Fellow, Faculty of Aerospace Engineering, Kluyverweg 1, 2629 HS Delft, M.J.Heiligers@tudelft.nl.
[3] Lecturer, School of Engineering, James Watt South Building, Glasgow, G12 8QQ. Matteo.Ceriotti@glasgow.ac.uk
[4] James Watt Chair, Professor of Engineering Science, School of Engineering, James Watt South Building, Glasgow, G12 8QQ, Colin.Mcinnes@glasgow.ac.uk

continuous data relay for rovers at high latitudes [10]. An example scientific application would be a pole-sitter mission at Venus to observe the dual polar vortexes present to better understand the motion and apparent rotational deceleration of Venus' atmosphere [11]. Based on these applications, this Note investigates planetary pole-sitter missions at Venus, Earth and Mars.

The structure of the Note is therefore as follows. In Section II, the system dynamics and pole-sitter model are described. In Section III, mission profiles for pole-sitters maintaining constant separation from the host planet are calculated, comparative results for Venus, Earth and Mars are presented, and the impact of solar sail degradation on such pole-sitters is quantified. In Section IV, the method used to find variable separation orbits to minimise mass use through direct multiple shooting is described and the resulting mission profiles are presented. The mass budgets for hybrid and pure-SEP pole-sitters are compared for a range of initial and payload mass configurations. Finally, in Section V, the orbit mass use results are generalised through a parametric analysis of the planetary mass and obliquity.

This Note's main aim is to understand the broad impact of the target planet on the efficacy of a pole-sitter mission. Key mission criteria will be mass use (for the impact on mission time on station and payload mass) and separation from target (for the impact on sensor resolution/scope and communications efficacy).

II. Pole-Sitter Model

The pole-sitter is modelled within the circular restricted three-body problem (CR3BP) where the Sun and the target planet are assumed to move in circular paths around their common centre of mass and the impact of the satellite on the motion of both the Sun and the target planet is neglected. Figure 1 shows the coordinate system used. A synodic reference frame is considered, centred at the Sun-planet centre of mass, with the x axis along the Sun-planet vector and the z axis perpendicular to their orbital plane. Coordinates in the synodic reference frame are dimensionless: the Sun-planet separation, the frame's angular velocity, ω, and the Sun-planet system mass, are normalized to 1. With the mass ratio $\mu = m_2/(m_1 + m_2)$, the location of the Sun and planet along the x axis become $-\mu$ and $1 - \mu$, respectively.

The basic idea of a pole-sitter satellite is that it remains directly above a planetary Pole at all times. This Note initially considers pole-sitters which maintain a constant planetary separation, d, and then pole-sitters which vary in separation, $d(t)$, over a year, where $t = 0$ is defined as the winter solstice. Note that due to the target planet's obliquity,

δ_{eq}, the pole-sitter's trajectory is constrained to a conical surface in the synodic reference frame. However, to an observer on the Pole, the satellite would always be directly at the zenith.

This Note follows the model described by Ceriotti and McInnes [8], which is summarised here for the reader. In the synodic reference frame, the pole-sitter's path is given by:

$$\boldsymbol{r}(t) = \begin{bmatrix} d(t)\sin\delta_{eq}\cos\omega t + (1-\mu) \\ -d(t)\sin\delta_{eq}\sin\omega t \\ d(t)\cos\delta_{eq} \end{bmatrix} \tag{1}$$

This path feeds into the dynamics of the CR3BP, which are given by:

$$\ddot{\boldsymbol{r}} + 2\boldsymbol{\omega} \times \dot{\boldsymbol{r}} = -\nabla U(\boldsymbol{r}) + \mathbf{a} \tag{2}$$

with U the effective potential

$$U(\boldsymbol{r}) = -\frac{(1-\mu)}{r_1} - \frac{\mu}{r_2} - \frac{x^2+y^2}{2} \tag{3}$$

Figure 1 defines the vectors $\boldsymbol{r}_1$ and $\boldsymbol{r}_2$. The thrust acceleration, $\mathbf{a}$, is either composed of the SEP acceleration only, $\mathbf{a}_T$, or of a combination of the SEP and solar sail, $\mathbf{a}_s$, accelerations:

$$\mathbf{a}_T = a_T\hat{\boldsymbol{u}}_T = \frac{T}{m}\hat{\boldsymbol{u}}_T \tag{4}$$

$$\mathbf{a}_s = \frac{1}{2}\beta_0\frac{m_0}{m}\frac{1-\mu}{r_1^2}\sqrt{g^2\,cos^2\,\alpha + h^2\,sin^2\,\alpha}\,cos\,\alpha\,\hat{\boldsymbol{m}} \tag{5}$$

with T the SEP thrust magnitude, m the spacecraft mass (with the subscript '0' indicating the initial mass at time $t = 0$), and $\hat{\boldsymbol{u}}_T$ and $\hat{\boldsymbol{m}}$ the unit vectors of the SEP and sail accelerations. The latter are described through the cone and clock angles, α and δ [8], for example, $\hat{\boldsymbol{u}}_T = [\cos\alpha_T \quad \sin\alpha_T\sin\delta_T \quad \sin\alpha_T\cos\delta_T]^T$. Furthermore, g and h are coefficients representing the impact of adding thin film solar cells (TFSC) necessary to power the SEP thruster onto the sail surface:

$$g = 1 + \tilde{r}_s + \frac{A_{TF}}{A}(\tilde{r}_{TF} - \tilde{r}_s) \tag{6}$$

$$h = 1 - \tilde{r}_s - \frac{A_{TF}}{A}(\tilde{r}_{TF} - \tilde{r}_s) \tag{7}$$

where the sail reflectivity $\tilde{r}_s = 0.9$, the TFSC reflectivity $\tilde{r}_{TF} = 0.4$ and the ratio of sail area covered by TFSC is $A_{TF}/A = 0.05$. Finally, the solar sail performance is expressed through the so-called lightness number β_0 (ratio of the solar radiation pressure acceleration to the solar gravitational acceleration), which is a measure of the solar sail

effectiveness. A value of $\beta_0 = 0.05$ is plausible for a near-term mission and a value of $\beta_0 = 0.1$ for a long-term mission [8]. Note that a value of $\beta_0 = 0$ corresponds to the use of SEP propulsion only.

Due to the consumption of SEP propellant, the satellite's mass profile follows

$$\dot{m} = -T/(I_{sp} g_0) \tag{8}$$

with I_{sp} the thruster's specific impulse and g_0 the standard gravity acceleration on the Earth's surface. The evolution of the pole-sitter state $\boldsymbol{x}$ can then be expressed in the following differential form

$$\dot{\boldsymbol{x}} = \begin{bmatrix} \dot{\boldsymbol{r}} \\ \dot{\boldsymbol{v}} \\ \dot{m} \end{bmatrix} = \begin{bmatrix} \boldsymbol{v} \\ -\boldsymbol{\nabla U} - 2\boldsymbol{\omega} \times \boldsymbol{v} + a_s \hat{\boldsymbol{m}} + a_T \hat{\boldsymbol{u}}_T \\ -T/(I_{sp} g_0) \end{bmatrix} \tag{9}$$

This Note considers a test satellite of mass at injection into the pole-sitter orbit of 1000 kg, including fuel, payload and propulsion, with other spacecraft details defined in Table 1. A more detailed mass budget as well as the effect of the initial mass on the mission performance is considered in Section III.C. Finally, Table 2 contains planetary parameters for the planets considered in this Note.

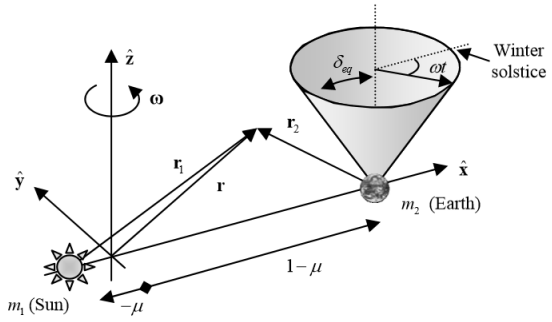

Figure 1 Diagram of pole-sitter motion within synodic reference frame [8].

Table 1 Satellite parameters

Parameter	Value(s)
Mass at orbital injection, kg	1000
β_0	0 (pure SEP), 0.05, 0.1
I_{sp}, s	3200

Table 2 Planetary parameters

	Venus	Earth	Mars
δ_{eq}, deg	-177.5	23.5	25.19
$\mu \cdot 10^6$	2.2416	3.0304	0.3233
Orbital radius, AU	0.7233	1	1.524
Orbital period, years	0.62	1	1.88

III. Constant Separation Pole-Sitters

This section starts the planetary pole-sitter analyses by assuming that the problem may be approximated as a pole-sitter orbiting at constant separation from the target planet. This assumption is retrospectively justified by the optimal trajectories presented in Section IV.

A. Approach

For a pole-sitter maintaining a constant separation, the trajectory is known from Eq. 1 and finding the control scheme becomes an inverse control problem. The objective is to find the control profile which minimizes the fuel usage over a complete orbit. Inverting the equations of motion (EoM) in Eq. (9) for a particular location along the pole-sitter path gives a unique required acceleration. For an SEP-only configuration, this required acceleration equals what is needed from the SEP thruster. Instead, for a hybrid configuration, the controls must be chosen such that this required acceleration is provided in the most fuel-efficient way. Starting at time $t = 0$, this is achieved by:

1. Using a sequential quadratic programming optimization method (implemented in the MATLAB® function *fmincon*) to orientate the sail, i.e. find the solar sail cone and clock angles, so as to minimize the thrust required from the SEP thruster at that instant.
2. Holding the rate of propellant use constant, advancing time by a small increment Δt and updating the remaining mass.
3. Repeating steps 1 to 2 until orbit is complete at time $t = 1$ planet-year.

B. Results

Figure 2 shows how the propellant mass per planet-year varies with separation, where the mass fraction is defined as $\frac{m(T)-m(0)}{m(0)}$. For each planet, there exists a unique "sweet spot" for mission lifetime where rotational and gravitational

forces best counterbalance. This point lies at a separation of 1.8 million km for Venus, 2.8 million km for Earth, and 2 million km for Mars, with little difference in the location of this sweet spot between the SEP-only and hybrid configurations. These plots are a useful resource for mission planners to balance fuel use and optimal separation, and to select which sensor and communications packages are most appropriate.

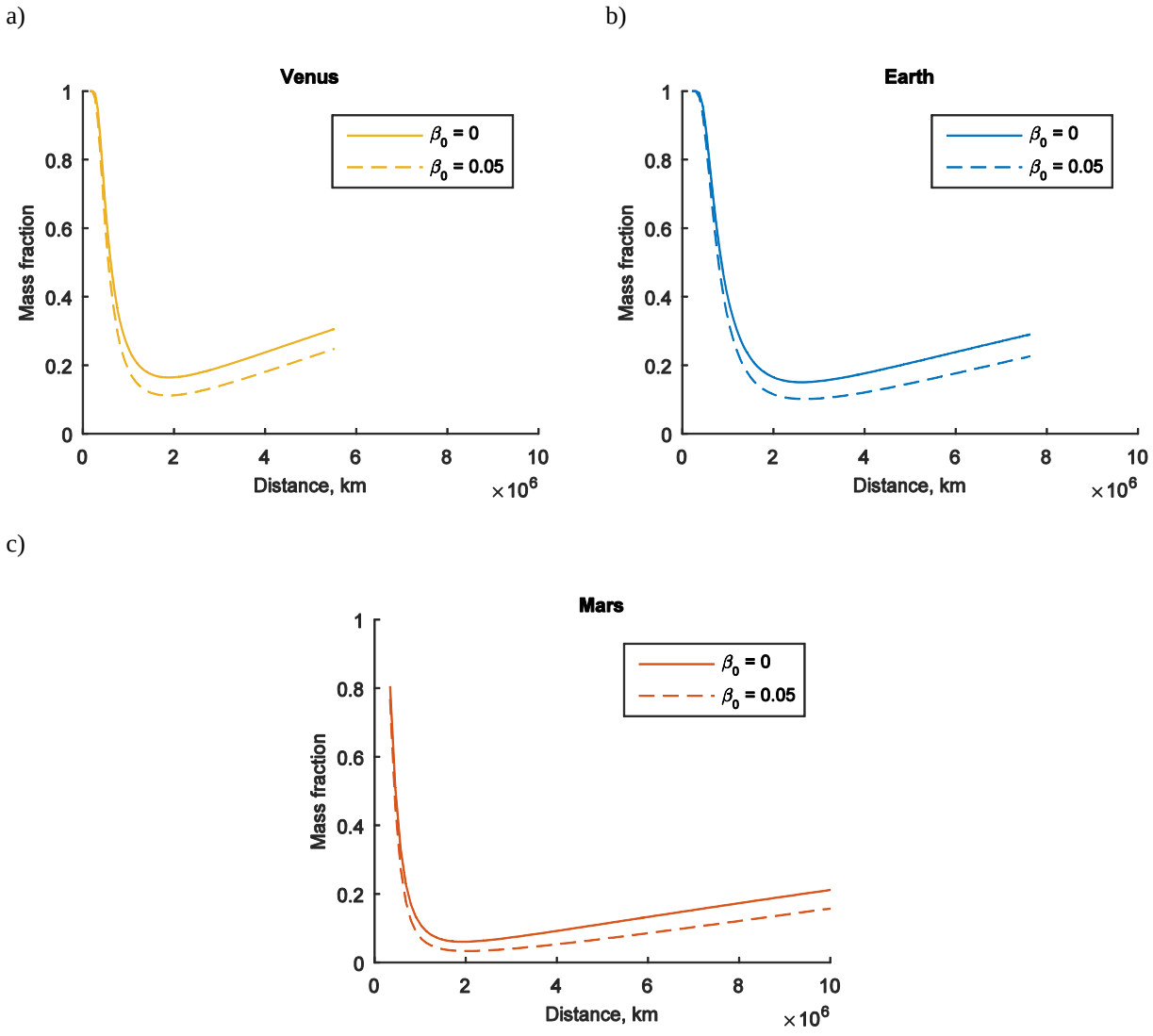

Figure 2 Mass fraction as a function of the constant separation distance for different solar sail lightness numbers, β_0 at a) Venus, b) Earth, and c) Mars.

Table 3 Mass remaining after complete orbit at Venus, Earth, Mars

	$\beta_0 = 0$	β_0=.05	$\beta_0 = .1$
Mass at Venus, kg	835.9	888.4	903.6
Mass at Earth, kg	849.7	898.8	903.5
Mass at Mars, kg	939.5	966.5	970.2

Table 3**Error! Reference source not found.** shows the mass use of a pole-sitter at the previously mentioned "sweet-spot" at Venus, Earth, and Mars. Significant mass savings are achieved using hybrid propulsion, but with diminishing returns for a given increase in β_0. This finding holds in all contexts considered within this Note, and will not be explicitly stated each time.

To aid mission planning, where mission lifetime is a key metric, Table 4 shows an estimate of the typical mass use per Earth-day:

$$Typical\ mass\ use\ = \frac{Total\ mass\ use\ per\ orbit}{Earth\ days\ per\ orbit} \tag{10}$$

Mars is found to offer the lowest mass use per unit time on station (an order of magnitude smaller compared to Venus) for all configurations, making it an attractive proposition for a complete launch-to-end mission design. Why Mars forms such a good candidate for a pole-sitter mission will be investigated in more detail in Section V.

Table 4 Typical mass used per Earth-day at Venus, Earth, Mars

	$\beta_0 = 0$	β_0=.05	$\beta_0 = .1$
Mass at Venus, kg/day	1.03	0.80	0.73
Mass at Earth, kg/day	0.59	0.45	0.41
Mass at Mars, kg/day	0.13	0.09	0.09

C. Mass budget analysis

The analyses so far have only compared the pure SEP and hybrid configurations based on the propellant consumption and only for the same mass at orbital injection, $m_0 = 1000$ kg. Although the latter is a realistic assumption (as shown in

Reference [3]), it would be useful to compare the configurations' performance based on the payload mass that can be carried onboard the pole-sitter spacecraft for a given lifetime of the mission. For this, a spacecraft mass budget analysis is performed, similar to the one presented in Reference [3] and details are therefore omitted here. For an SEP spacecraft, a range of spacecraft subsystems are taken into account, including the thruster mass, the propellant tank mass, the mass of the solar arrays required to provide adequate levels of power to the SEP thrusters as well as the propellant mass and the payload mass. An appropriate margin of five percent is added to all of these components, except the payload mass. For the hybrid configuration, additional mass components are included in this mass budget analysis to account for the mass of the solar sail. Furthermore, the solar arrays of the SEP spacecraft are replaced by the more mass-efficient TFSC, which in turn require the addition of radiators to dissipate excess power as the power generated by the TFSC is constrained by the solar sail's attitude. A larger margin of ten percent is applied to the solar sail and the TFSC as these are considered to be new technologies.

The results of this mass budget analysis are provided in Figure 3. These results show the mission performance in terms of pole-sitter altitude (once again clearly showing the existence of "sweet spot" altitudes), mission lifetime, payload mass and initial mass. Solid and dashed lines are for the SEP and hybrid configurations ($\beta_0 = 0.05$), respectively. The results on the left hand side of the figure (subplots a, c, and e) assume an initial spacecraft mass of $m_0 = 1000$ kg and vary the payload mass, m_{pay} . Clearly, the larger m_{pay}, the shorter the mission lifetime for a given pole-sitter altitude. Instead, the results on the right-hand side of Figure 3 (subplots b, d, and f) assume a particular payload mass, $m_{pay} = 100$ kg and show what the initial mass of the spacecraft would have to be to carry that payload mass. These results show that, the larger the initial mass, the longer the mission lifetime (at least for the values for m_0 considered here).

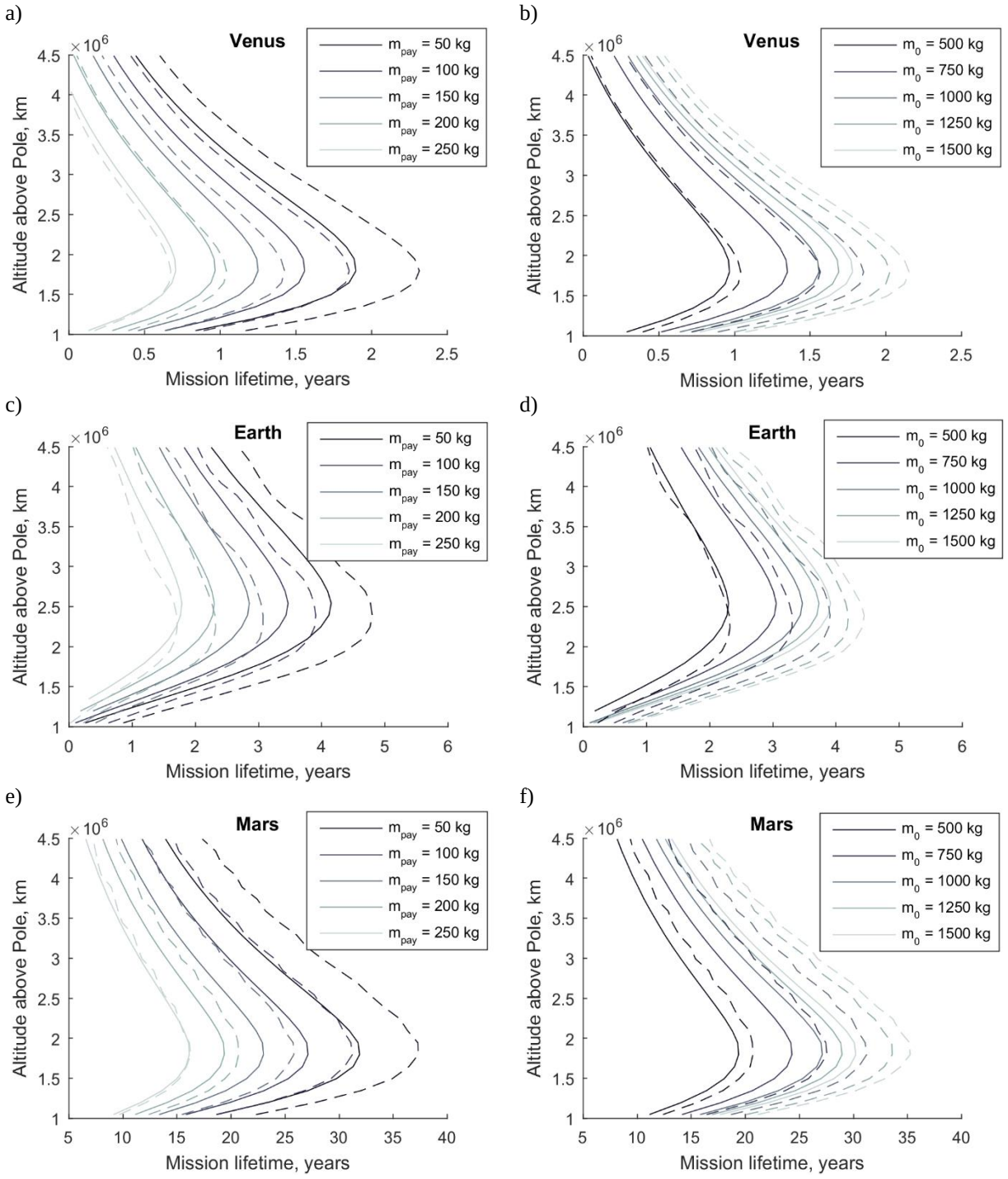

Figure 3 Spacecraft mass budget results for constant separation pole-sitters at Venus, Earth and Mars. Solid and dashed lines are for the pure SEP and hybrid configurations (β_0 = 0.05), respectively. a, c, e) Available payload mass, m_{pay}, for an initial spacecraft mass of m_0 = 1000 kg. b, d, f) Required initial mass, m_0, for a payload mass of m_{pay} = 100 kg.

Figure 3 shows an interesting result, namely that the hybrid configuration does not always outperform the SEP-only configuration even though the propellant consumption may indicate otherwise. While the hybrid configuration *does* outperform the SEP-only configuration for pole-sitters at Mars, it only provides a gain in mission performance for pole-sitters at Venus and Earth for small payload masses or large initial masses. For larger payload masses or smaller initial masses the addition of a solar sail with $\beta_0 = 0.05$ does not outweigh the propellant savings and smaller values for the lightness number will have to be considered to achieve better performances. Note, however, that it is not just a matter of finding the breakeven point between propellant consumption and solar sail mass. For example, the difference in the power generating systems (solar arrays versus TFSC) and the addition of radiators for the hybrid case need to be considered, as well as other effects. For example, adding a solar sail may lower the peak SEP thrust, which will downsize the solar array and SEP thruster mass compared to the SEP-only configuration.

Finally, Figure 3 shows wavy patterns in the results for hybrid pole-sitters at Earth and Mars. Such wavy patterns are created by seasonal variations in the required acceleration to maintain the pole-sitter orbit due to the tilt of the polar axis. Moreover, for the hybrid case, part of this acceleration is provided by the solar sail and the sail's contribution varies highly along the orbit. As a result, the propellant consumption varies, which in turn produces the wavy patterns in Figure 3. Because Venus' polar axis is almost perpendicular to its orbital plane (see Table 2), these seasonal variations occur to a much lesser extend (the required acceleration and contribution of the sail are almost constant along the orbit). Therefore, the wavy patterns observed for hybrid pole-sitters at Earth and Mars are not present in the results for Venus.

D. Solar Sail Degradation

The previous analysis applies a solar sail model that implicitly neglects sail degradation (see Eq. (5)). In this section, that assumption is qualitatively investigated. The impact of solar sail degradation is modelled following Dachwald et al. [12]. The sail decay is modelled through an exponential decay of the lightness number based on the total accumulated solar radiation dose, $\Sigma(t)$:

$$\beta(t) = \beta_0 \frac{1 + De^{-\lambda \Sigma(t)}}{1 + D} \tag{11}$$

with D the degradation factor and λ the degradation constant.

Figure 4**Error! Reference source not found.** shows the degradation effect on propellant use for $D = 1$ over many possible λ values. The figure highlights that the hybrid propulsion configuration outperforms the SEP-only configuration in terms of propellant consumption over a range of possible λ.

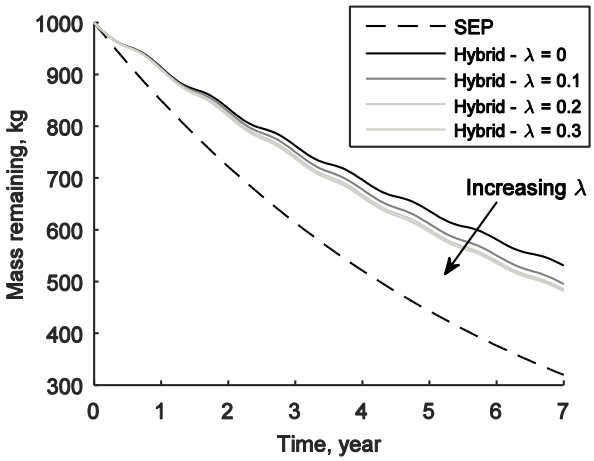

Figure 4 Impact of sail degradation on mass profile for an Earth pole-sitter mission.

IV. Optimal Trajectory Pole-Sitters

It is possible to achieve significant mass savings by varying the separation $d(t)$ of the satellite over the year. These fuel-optimal ('optimal' hereafter) trajectories allow for longer mission times and therefore greater scientific or technical returns. For finding these optimal trajectories, the inverse control problem method used in the constant separation case is no longer applicable since d now becomes a function of time, $d(t)$, where $d(t)$ is the unknown path function. Since the path is not known a priori, it cannot be inverted to find the required acceleration at each point through the EoM. A different method must therefore be used that finds both optimal path and controls such that fuel usage is minimized over a complete orbit whilst remaining above the Pole.

A. Direct Multiple Shooting

Optimal trajectories and control profiles are found with a direct multiple shooting (DMS) scheme [13]. The semi-analytic solution for a pole-sitter maintaining a constant separation (see Section III) provides a suitable initial guess to seed the DMS scheme. By interpolating the states and controls found for a constant separation pole-sitter, the functions $\boldsymbol{x}_n$, $\mathbf{a}_{s,n}(t)$ and $\mathbf{a}_{T,n}(t)$ are found for each segment that, when integrated, give a constant separation pole-sitter trajectory where $\boldsymbol{x}(t_{n+1}) = \boldsymbol{x}_0(t_{n+1})$. This initial feasible set of states and controls can then be adjusted at each node to minimize the propellant consumption while satisfying 4 sets of constraints:

1. Continuity of states between segments $\boldsymbol{x}(t_{n+1}) = \boldsymbol{x}_0(t_{n+1})$, as outlined above.
2. Orbit periodicity: to find orbits suitable for multi-year missions, continuity of initial and final states $\boldsymbol{x}_0(t_0) = \boldsymbol{x}_f(t_f)$ is required (with the exception of final mass) such that the orbit may be repeated while propellant remains.
3. Pole-sitter trajectory: the satellite must follow the path $\boldsymbol{r}(t)$ described by Eq. (1).
4. Continuity of controls: this is not mathematically required as a system with continuous well-behaved dynamics ought to have optimal trajectories with smooth control profiles. However, explicitly requiring this condition helps inform how $\boldsymbol{a}_{s,n}(t)$ and $\boldsymbol{a}_{T,n}(t)$ are iterated, thereby improving convergence.

The resulting non-linear programming problem is iterated on using *fmincon*. The variables to be optimised by *fmincon* are composed of 3 types:

1. For each segment, an initial state value $\boldsymbol{x}_0(t_n)$ setting the segment integration initial conditions on the position and velocity coordinates and the mass.
2. For each segment, the coefficients of an $\boldsymbol{a}_{s,n}(t)$ polynomial function controlling the sail orientation angles $\alpha_s(t)$ and $\delta_s(t)$ [8].
3. For each segment, the coefficients of an $\boldsymbol{a}_{T,n}(t)$ polynomial function controlling the SEP acceleration components in Cartesian coordinates.

Manual scaling is used such that all initial constraint violations are of the same order. The DMS scheme divides the orbit into 14 segments and typical optimisations take between 400 and 2000 iterations to converge.

B. Results

The final results for an Earth-based pole-sitter independently identify the results found in [2], which adopted a direct pseudo-spectral method, thus corroborating one another and allowing for a future comparative study between different numerical optimal control methods.

Optimal trajectories generated for pole-sitters at Venus and Mars are shown in Figure 5 and Figure 6. In all cases, significant mass savings are achieved in comparison with the constant separation approximation considered earlier in this work, see Table 3 and Table 5**Error! Reference source not found.**. Note that the results in Table 5 for the constant separation pole-sitter once again assume an altitude at the previously established ‘sweet spots’, see Section III.B.

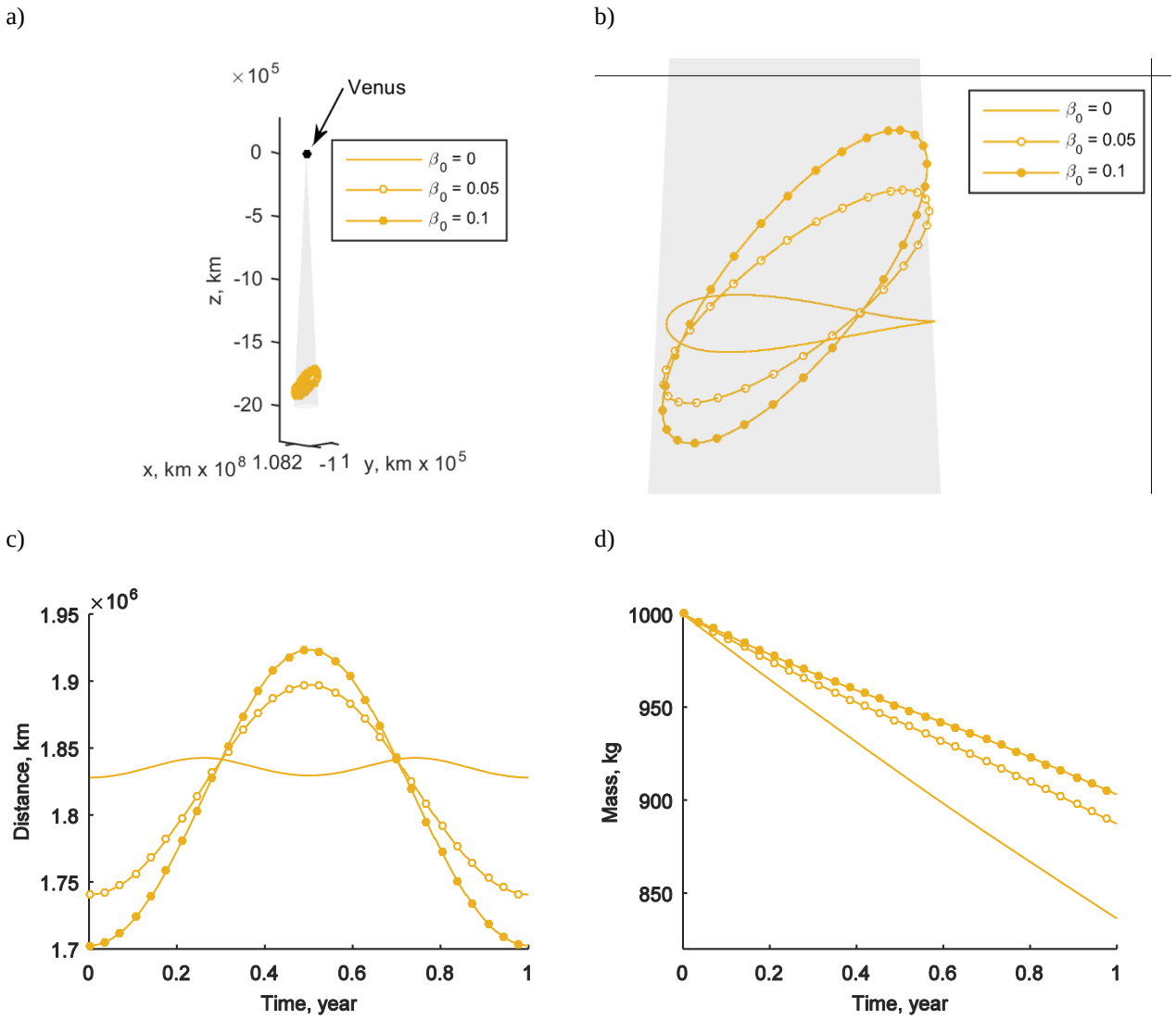

Figure 5 Optimal Venus pole-sitter mission. a) Trajectories – wide view. b) Trajectories – narrow view. c) Distance profile. d) Mass profile.

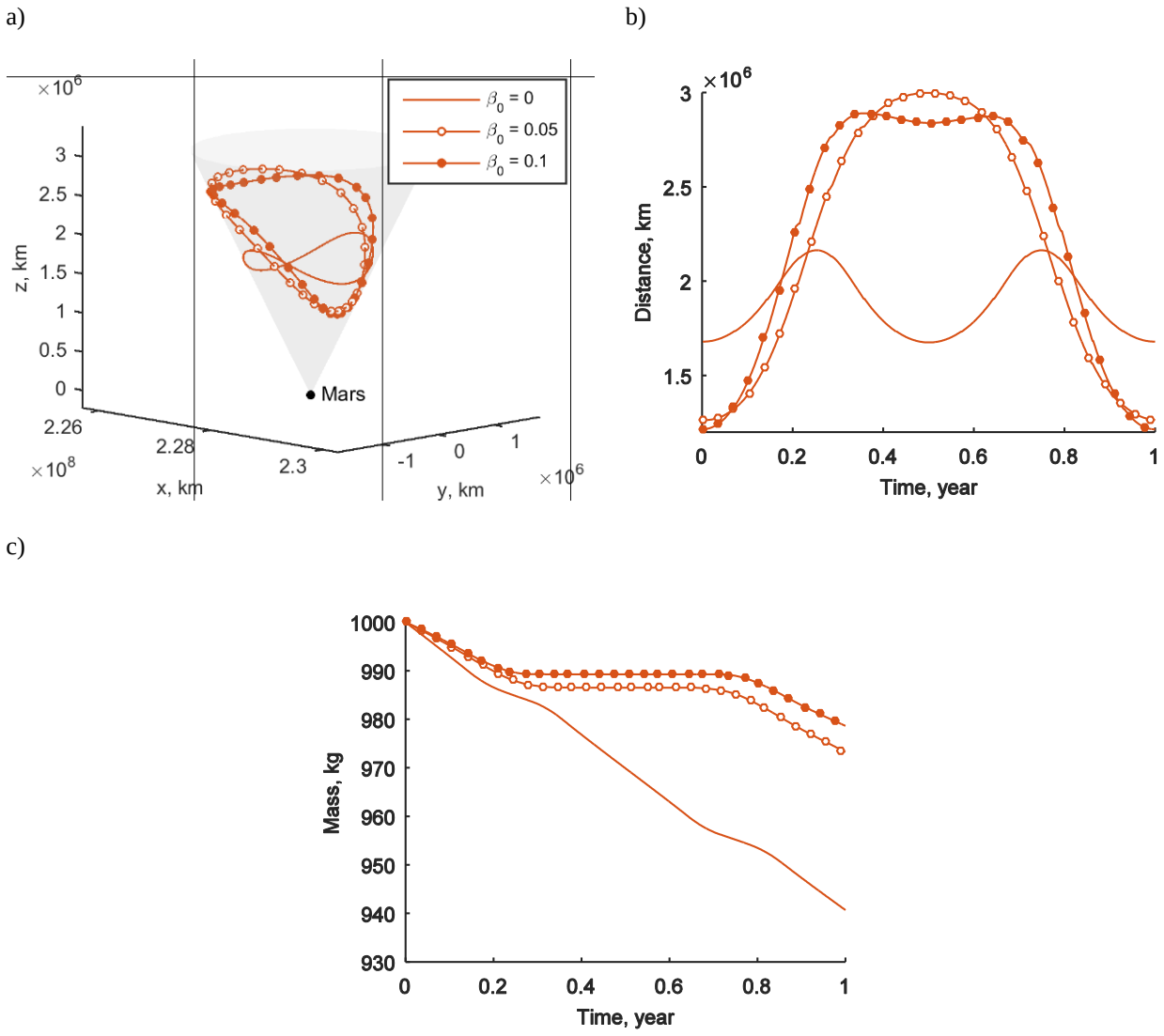

Figure 6 Optimal Mars pole-sitter mission. a) Trajectories. b) Distance profile. c) Mass profile.

For all three planets, the SEP-only ($\beta_0 = 0$) optimal orbits achieve maximum separation at $t = 0.25$ and 0.75. This is consistent with the results found for Earth by Ceriotti and McInnes [8]. The physical explanation for this apparent principle is not yet known. The optimal orbits found when hybrid propulsion is used ($\beta_0 = 0.05$ and 0.1) have peak separation during the summer solstice. In this case, the physical explanation is that the sail can be best used to counteract the gravitational acceleration of the planet in this part of the trajectory. When the satellite is between planet and Sun, the sail acceleration vector may be used to give the greatest acceleration out of the ecliptic plane. The sail is least effective along the z axis during the winter solstice. Increasing the separation magnifies these effects. The optimiser therefore

chooses to maximise separation when the sail is most effective (summer solstice) and minimise separation when the sail is least effective (winter solstice).

Table 5 Typical mass use per Earth-day for optimal separation pole-sitter orbits

	$\beta_0 = 0$	$\beta_0 = .05$	$\beta_0 = .1$
Mass at Venus, kg/day	0.72	0.50	0.43
Mass at Earth, kg/day	0.40	0.26	0.20
Mass at Mars, kg/day	0.09	0.04	0.03

Finally, similar to the mass budget analysis in Section III.C for the constant separation pole-sitter, Figure 7 presents the mission performance in terms of the payload mass and mission lifetime for the optimal pole-sitter orbits at Venus, Earth and Mars, considering a range of initial spacecraft masses. The results show a behaviour similar to that in Figure 3 for the constant separation pole-sitters: the hybrid configuration (with $\beta_0 = 0.05$) does not always outperform the SEP-only configuration even if the propellant consumption may indicate otherwise. Especially for Venus and Earth it becomes clear that only for longer mission lifetimes and larger initial masses the hybrid configuration outperforms the SEP-only configuration. Better performances for shorter lifetimes and smaller initial masses may again be obtained when considering smaller values for the sail's lightness number. Finally, note that the break-even point between the two configurations occurs at a specific mission lifetime for every initial mass considered due to the fact that the achievable payload mass scales linearly with the initial mass.

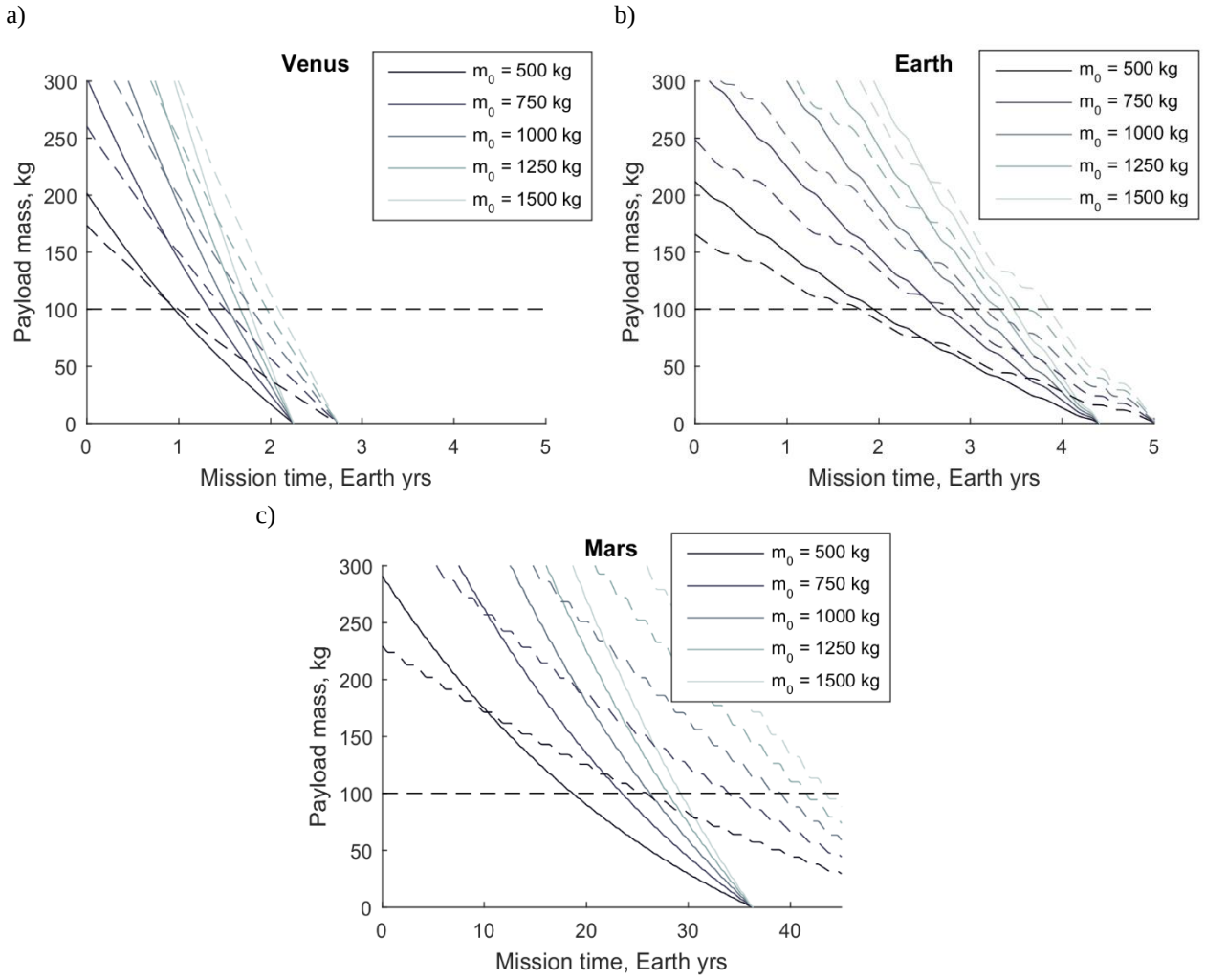

Figure 7 Spacecraft mass budget results for optimal pole-sitters at a) Venus, b) Earth and c) Mars. Solid and dashed lines are for the pure SEP and hybrid configurations (β_0 = 0.05), respectively.

V. Parametric Analysis

So far, this Note has only considered three discrete test cases, i.e. Earth, Venus and Mars, with Mars requiring the smallest typical mass use per day. To further investigate why Mars appears to be a good candidate for a pole-sitter mission and to gain a physical understanding of what determines how efficient the maximally-optimal trajectory at a given planet will be, this section considers a parametric analysis on the Sun-planet system's mass ratio, obliquity and distance from the Sun. These three parameters are chosen as they fully define the pole-sitter dynamics within the framework of the CR3BP. The mass ratio is required because the station-keeping acceleration required to maintain the

pole-sitter non-Keplerian orbit significantly depends on the gravitational potential close to the target planet. Obliquity is required because it describes how the distance of the satellite to each primary body varies throughout the year, with a time dependency introduced as the obliquity increases from 0.

A. Constant Separation

Table 5 shows that the mass savings obtained for the optimal pole-sitter compared to the constant separation pole-sitter are smaller than the difference in propellant mass use between different planets. The constant separation approximation can therefore be used to quickly obtain insights in the relative ease with which the pole-sitter orbit can be maintained at different planets.

Figure 8 shows the results of the parametric analysis which considers a constant separation distance of 0.01 AU and a mission time of 1 Earth-year. The left column provides the final mass for the SEP-only configuration, while the right column provides the mass savings that can be achieved with the hybrid configuration for a lightness number of $\beta_0 = 0.1$. For each configuration, three Sun-planet distances are considered (those of Venus, Earth, and Mars) as well as a range of values for the obliquity and mass ratio, μ. The true values of these parameters for Venus, Earth, and Mars are indicated with a marker.

The results for the SEP-only configuration show the following: the closer to the Sun, the smaller the spacecraft final mass. Furthermore, the farther from the Sun, the more important the mass ratio becomes (the lower, the better), while the importance of the obliquity diminishes. Mars is therefore a good candidate for a pole-sitter mission as it orbits far from the Sun, with a low mass ratio. Its obliquity is of almost no importance.

When looking at the results for the hybrid configuration, it becomes clear that, the closer to the Sun, the larger the absolute gain in final mass is. However, this increased gain does not outweigh the poorer performance of the SEP-only configuration closer to the Sun. Furthermore, for planets close to the Sun, the obliquity is clearly most important (with values around 45 deg performing best), while for planets far from the Sun, the mass ratio is once again most important. Although Venus provides the largest absolute gain in final mass, Earth seems to be a better option in a relative sense as its obliquity and mass ratio allows the greatest mass savings at Earth-distance, while the opposite holds true for Mars.

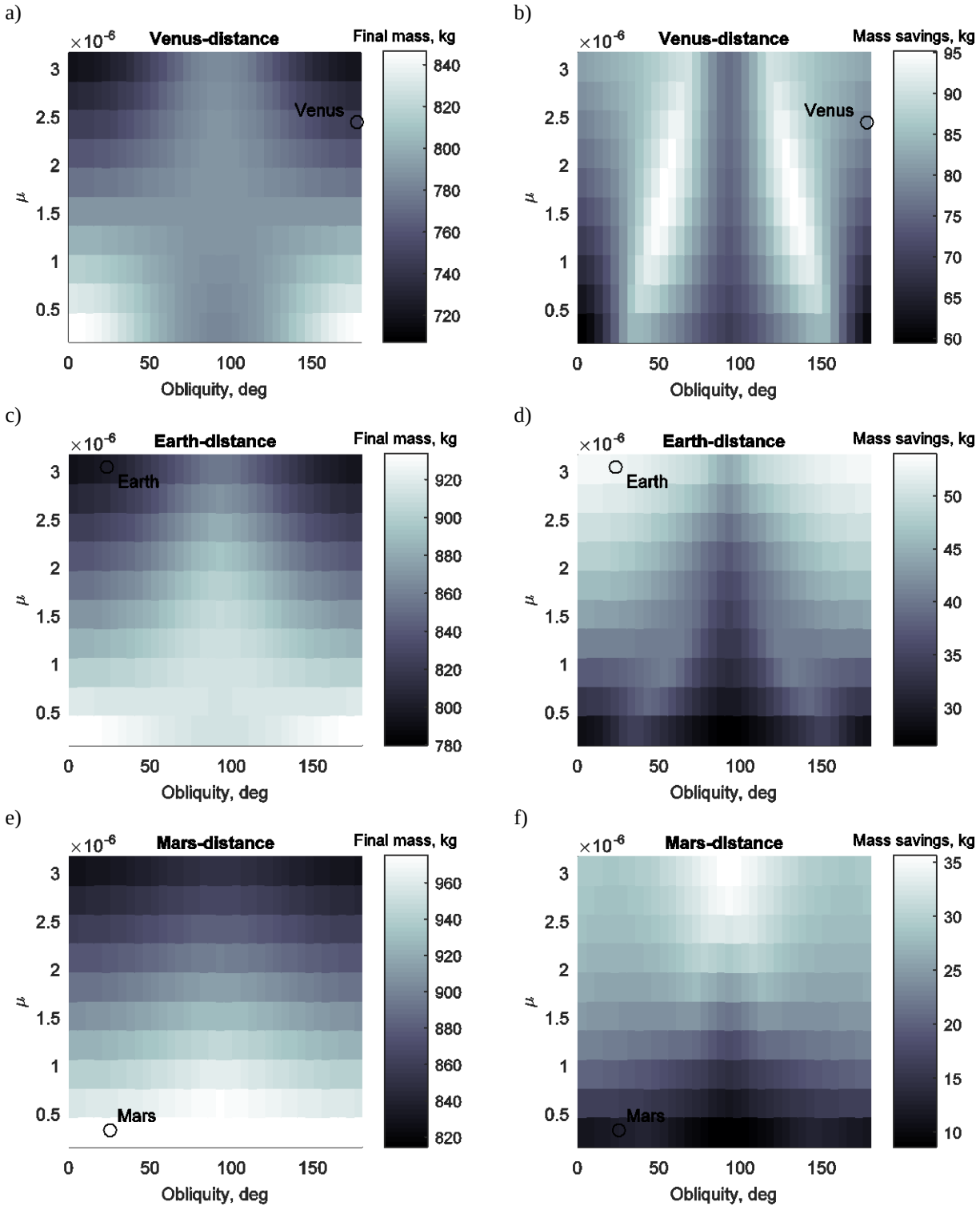

Figure 8 Parametric analysis for constant separation pole-sitters. a, c, e) Final mass for SEP-only configuration at Venus, Earth, and Mars distances. b, d, f) Mass savings for hybrid propulsion ($\beta_0 = 0.1$) at Venus, Earth, and Mars distances.

B. Optimal Trajectory

Extending the analysis in the previous section to the optimal trajectory pole-sitter, the results in Figure 9 can be obtained. Due to the computational effort involved, the parameter space is reduced to a smaller range in the obliquity and only Earth's distance to the Sun is considered. Where extreme values of the obliquity and mass ratio caused the DMS scheme of Section IV.A to fail, white space is plotted, representing no available data. The figure shows very similar results as in Figure 8c,d: where the system has a large mass ratio, a low axial is favoured, and as μ decreases, the obliquity becomes less significant. Overall, it is clear that also for the optimal pole-sitter, μ is the dominant determinant for the fuel efficiency. This explains once again why, the fuel consumption values for Mars are significantly smaller than those for Earth or Venus.

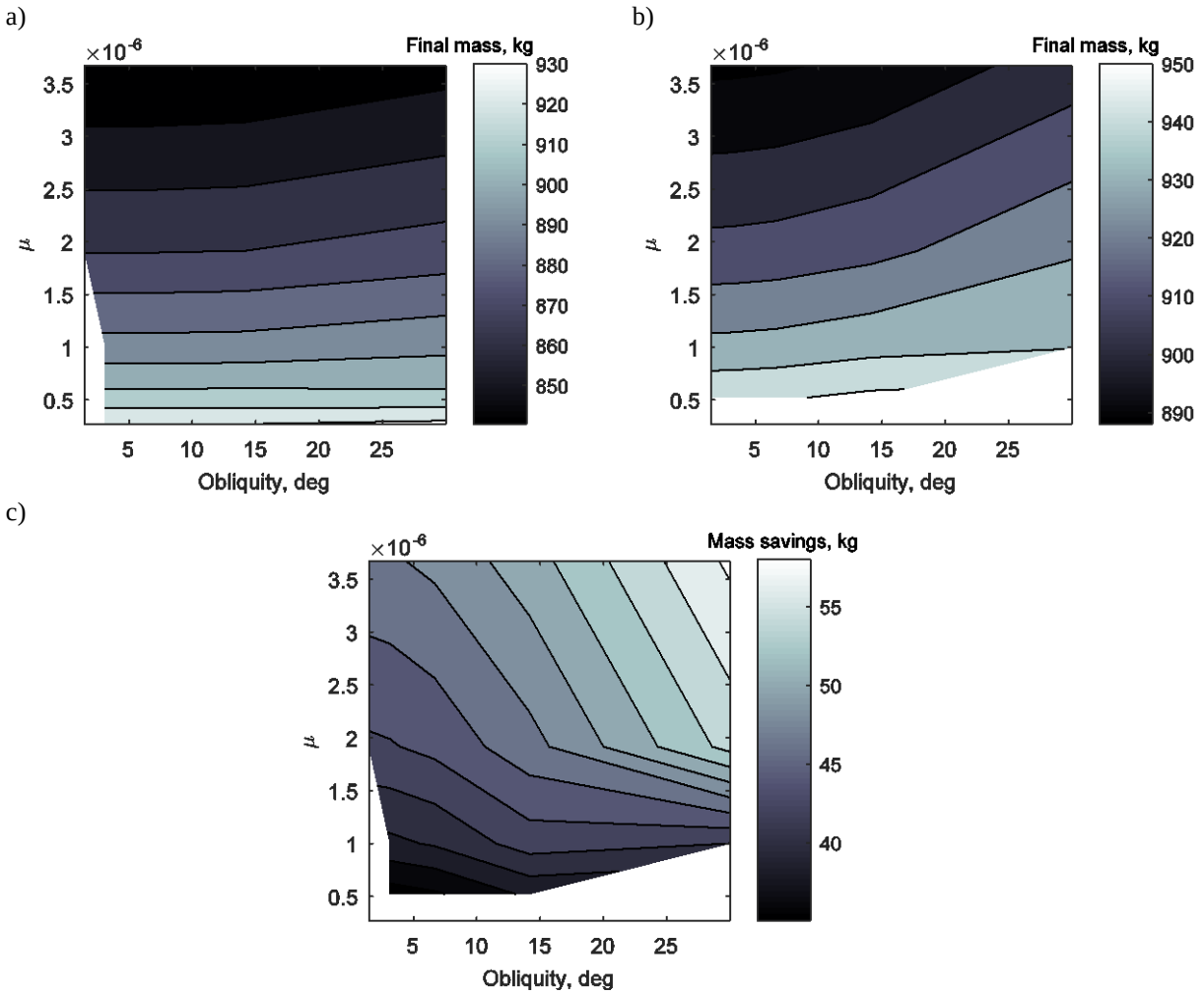

Figure 9 Parametric analysis for optimal pole-sitters at 1 AU. a) Final mass for SEP-only configuration. b) Final mass for hybrid propulsion, $\beta_0 = 0.05$. c) Mass savings by hybrid propulsion.

VI. Conclusions

This Note has extended previous work on the concept of an Earth pole-sitter mission to other inner Solar System planets. When comparing the fuel efficiency for the case where the planet-satellite distance is kept constant, a Martian pole-sitter mission is found to be dramatically more fuel-efficient than one at Earth or Venus. This is due to its far distance from the Sun as well as due to the Sun-Mars system's mass ratio. A Martian pole-sitter mission also allows for smaller planet-satellite distances, making it a strong candidate for an end-to-end mission analysis. When comparing the performance of an SEP-only configuration and a hybrid SEP + solar sail configuration, the hybrid configuration always outperforms the SEP-only configuration from a fuel efficiency point of view. Even if solar sail degradation is included, which may lead to significantly increased fuel consumption, the hybrid craft remain more fuel-efficient than SEP-only satellites, even with very high sail degradation rates. However, when expressing the mission's performance in terms of the payload mass that can be accommodated on-board for a particular mission lifetime it becomes clear that the hybrid configuration (for the lightness numbers considered in this paper) only fully outperforms the SEP-only configuration for a pole-sitter at Mars, while for pole-sitters at Venus and Earth similar superior performances are only observed for small payload masses or large initial masses.

When allowing the planet-satellite distance to vary over time, optimal Earth trajectories have been generated using a direct multiple shooting scheme. These are found to corroborate previous results found with a direct pseudo-spectral method, allowing for a future comparative study between different numerical optimal control methods. Extending these optimal pole-sitter trajectories from Earth to Venus and Mars shows a recurring shape of maximum planet-satellite distances at summer solstice for a hybrid craft, which is explained by the fact that the sail can provide a maximum out-of-ecliptic acceleration at summer solstice. When comparing the performance of the SEP-only and hybrid configurations for these optimal pole-sitter trajectories, the hybrid configuration is once again more fuel-efficient that the SEP-only option, but from a spacecraft mass analysis it again becomes clear that the hybrid configuration only outperforms the SEP-only option for longer mission lifetimes and larger initial masses.

Finally, a parametric analysis on the planet's mass and obliquity has been conducted, which enabled an investigation into the general physical principles for optimal orbit efficiency. It is shown that both for the constant separation as well as for the optimal pole-sitter, the planet's mass is the dominant factor, with the planet's obliquity playing a significant role only for planets close to the Sun and for the hybrid, optimal trajectory pole-sitter at high mass planets.

VII. Acknowledgements

M. Walmsley would like to thank Joe Bradley, Peter Fockema, Elizabeth Tatham and Andrew Mackie for their input on solar sail decay, Agne Skripkaite and the Edinburgh University Young Scientific Researchers Association (EUSYRA) for organizational support and the British Interplanetary Society (BIS) and the Royal Aeronautical Society (RAS) for financial support. C.R. McInnes and J. Heiligers would like to acknowledge the support from the European Research Council Advanced Investigator Grant-227571: Visionary Space Systems: Orbital Dynamics at Extremes of Spacecraft Length-Scale. Finally, J. Heiligers would also like to acknowledge the support from the Marie Skłodowska-Curie Individual Fellowship 658645 - S4ILS: Solar Sailing for Space Situational Awareness in the Lunar System.

VIII. References

[1] Driver, J., "Analysis of an Arctic Polesitter spacecraft in stationary orbit," *17th Aerospace Sciences Meeting*, New Orleans: 1979. doi: 10.2514/6.1979-127

[2] Heiligers, J., Ceriotti, M., McInnes, C. R., and Biggs, J. D., "Mission analysis and systems design of a near-term and far-term pole-sitter mission," *Acta Astronautica*, vol. 94, Jan. 2014, pp. 455–469.

[3] Ceriotti, M., Heiligers, J., and McInnes, C., "Trajectory and Spacecraft Design for a Pole-Sitter Mission," *Journal of Spacecraft and Rockets*, vol. 51, Jan. 2013, pp. 311–326.

[4] McInnes, C. R., *Solar Sailing: Technology, Dynamics and Mission Applications*, pp. 32-40. Berlin: Springer Praxis Books, 2004.

[5] Mori, O., Sawada, H., Funase, R., Morimoto, M., Endo, T., Yamamoto, T., Tsuda, Y., Kawakatsu, Y., Kawaguchi, J., Miyazaki, Y., Shirasawa, Y., and Demonstration Team and Solar Sail W, I., "First Solar Power Sail Demonstration by IKAROS," *Transactions of the Japan Society for Aeronautical and Space Sciences, Aerospace Technology Japan*, vol. 8, 2010, pp. 425–431.

[6] Johnson, L., Whorton, M., Heaton, A., Pinson, R., Laue, G., and Adams, C., "NanoSail-D: A solar sail demonstration mission," *Acta Astronautica*, vol. 68, 2011, pp. 571–575.

[7] Biddy, C., and Svitek, T., "LightSail-1 Solar Sail Design and Qualification," *Proceedings of the 41st Aerospace Mechanisms Symposium*, Los Angeles: 2012, pp. 451–463.

[8] Ceriotti, M., and McInnes, C. R., "Generation of Optimal Trajectories for Earth Hybrid Pole Sitters," *Journal of Guidance, Control, and Dynamics*, vol. 34, May 2011, pp. 847–859.

[9] Walmsley, M., "Trajectory Design for Planetary Polesitter Missions," *65th International Astronautical Congress* IAC-15-E2.2.7, Israel: 2015.

[10] McKay, R., Macdonald, M., Bosquillon de Frescheville, F., Vasile, M., McInnes, C., and Biggs, J., "Non-Keplerian orbits using low thrust, high isp propulsion systems," *60th International Astronautical Congress* IAC-09-C1.2.8, Korea: 2009.

[11] Schubert, G., Covey, C., Del Genio, A., Elson, L. S., Apt, J., Kliore, A. J., Keating, G., Seiff, A., and Young, R. E., "Structure and circulation of the Venus atmosphere," *Journal of Geophysical Research*, vol. 85, 1980, pp. 8007–8025.

[12] Dachwald, B., Mengali, G., Quarta, A. a., and Macdonald, M., "Parametric model and optimal control of solar sails with optical degradation," *Journal of Guidance, Control, and Dynamics*, vol. 29, 2006, pp. 1170–1178.

[13] Rao, A., "A survey of numerical methods for optimal control," *Advances in the Astronautical Sciences*, vol. 334, 2009, pp. 497–528.